Towards a fiber-coupled picowatt cryogenic radiometer

N. A. Tomlin,* J. H. Lehman, and S. Nam

National Institute of Standards and Technology, 325 Broadway, Boulder, Colorado 80305, USA
**Corresponding author: ntomlin@boulder.nist.gov*

Received February 15, 2012; revised March 27, 2012; accepted April 2, 2012;
posted April 3, 2012 (Doc. ID 163098); published June 11, 2012

A picowatt cryogenic radiometer (PCR) has been fabricated at the microscale level for electrical substitution optical fiber power measurements. The absorber, electrical heater, and thermometer are all on a micromachined membrane less than 1 mm on a side. Initial measurements with input powers from 50 fW to 20 nW show a response inequivalence between electrical and optical power of 8%. A comparison of the response to electrical and optical input powers between 15 pW to 70 pW yields a repeatability better than $\pm 0.3\%$ ($k = 2$). From our first optical tests, the system has a noise equivalent power of $\approx 5 \times 10^{-15}$ W/$\sqrt{\mathrm{Hz}}$ at 2 Hz, but simple changes to the measurement scheme should yield an NEP 2 orders of magnitude lower.

OCIS codes: 120.3930, 120.4800, 120.5630, 040.3780.

State-of-the-art cryogenic radiometers (CRs) at the National Institute of Standards and Technology and other national metrology institutes can calibrate optical power levels down to 1 μW with low uncertainties [1,2]. However, there are many emerging industries that use detectors and sources operating at much lower power levels, whose calibration typically requires a chain of measurements to tie to existing primary detector standards or high dynamic range source standards that are not widely available [3,4]. Though there are ongoing efforts to improve sensitivity at lower power levels by pushing existing fabrication methods to make CRs smaller, such approaches are difficult and unlikely to provide revolutionary improvements [5–7].

Instead of using conventional fabrication methods to push CRs to smaller sizes, we have instead taken a different approach and designed a radiometer fabricated lithographically at the microscale level [8]. The picowatt cryogenic radiometer (PCR) is designed to measure power levels on the order of 1 pW, many orders of magnitude lower power than current CRs. The lithographic fabrication opens many opportunities for microscale radiometers and applications that use them. For example, hundreds of identical devices can be fabricated on a single wafer, which is desirable for intercomparisons and dissemination to other metrology institutes. Alternatively, multiple variations in the design of the radiometer can be produced on the same wafer.

All CRs require a thermometer, an electrical heater, and an absorber to be in good thermal contact with each other, but isolated from the environment by a weak thermal link. In the present PCR, all components except for the absorber are fabricated lithographically on a silicon wafer (Fig. 1). The weak thermal link is provided by a silicon-nitride membrane, which suspends the remaining radiometer components and separates them from the bulk silicon of the device chip. The membrane is defined using silicon micromachining. A portion of the bulk Si is left underneath the center of the membrane to help thermalize all parts of the radiometer [Fig. 1(c)]. The thickness of the Si thermalizer is reduced from a starting wafer thickness of 400 μm to 200 μm to keep from thermally shorting the device when placed on a flat surface. The membrane thickness is 900 μm and hasa measured thermal conductance (G) of $\approx$740 pW/K at 12 mK.

The thermometer is a thin-film superconducting transition-edge sensor (TES), which is biased in the superconducting transition using negative electrothermal feedback [9]. The steep change in resistance versus temperature at the superconducting critical temperature (T_c) makes the TES an extremely sensitive thermometer. The TES consists of a 250 μm-square bilayer of Mo and Cu, with a T_c of 140 mK and a normal-state resistance (R_n) of $\approx$13 mΩ [10]. A 50 μm-diameter hole in the center of the TES, originally intended for an integrated absorber, was not used for this work. The TES is voltage-biased with a shunt resistor of $\approx$220 $\mu\Omega$, and the current is read out by a two-stage superconducting quantum interference device (SQUID) and commercially available electronics [11].

The electrical heater is a thin-film PdAu trace surrounding the TES with a resistance of 4.451 kΩ at the operating temperature, measured with a commercial resistance bridge. Joule heating in the resistor heats the membrane for the electrical substitution measurement. Electrical powers are applied to the heater using a

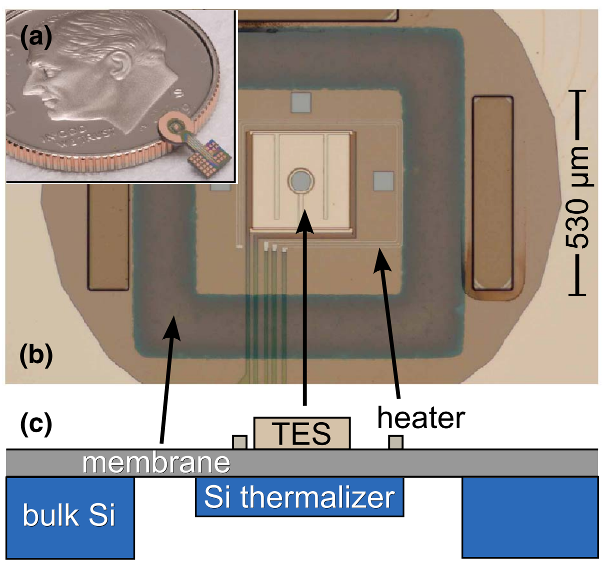

Fig. 1. (Color online) (a) Photograph of PCR chip (without the absorber) next to a dime for scale. (b) Photograph of the center of the PCR chip showing the membrane, thermometer, and heater (no absorber). (c) Side-view schematic of (b).

battery-powered voltage source and large bias resistor (≈10 MΩ) in series, while monitoring the voltages of the source and across the resistor. The thin-film wiring leads to both the heater and TES are superconducting Mo, so heating from the leads is assumed to be negligible.

Unlike conventional radiometers, which typically use a trap or cavity design with multiple reflections to ensure near-unity optical absorption, the PCR is limited to a small planar area. In lieu of a cavity, we have chosen to use multiwall carbon nanotubes (MWCNTs) as the absorber, because of their high absorption over a wide wavelength range [12]. The MWCNTs are attached to the surface of the TES using a two-part epoxy, which is applied with a micromanipulator. On separate macroscopic samples, we measured the total reflectance using an integrating sphere coupled to a spectrophotometer, which we used to infer absorption values of >97% for the MWCNTs and >93% for the epoxy between 350 nm and 2550 nm. Incident radiation is coupled to the absorber through a standard 9 μm core, single-mode telecommunication fiber. The outer perimeter of the PCR chip is etched in the shape of a partial circle so that it fits inside of a fiber sleeve, aligning the optical fiber tip to the center of the TES [Fig. 2(a)]. Known optical powers are applied with a 1550 nm CW fiber diode laser attenuated by three programmable fiber attenuators, which are calibrated using an optical switch and a powermeter [4].

The PCR is operated at a temperature of ≈12 mK in a dilution refrigerator [Fig. 2(b)]. Example TES current versus voltage (I-V) curves are shown in Fig. 3. During operation of the PCR, the TES thermometer is biased low in the superconducting transition and operated in a flux-locked loop in order to linearize the SQUID output [11]. For characterization purposes, instead of using electrical substitution to determine each applied optical power, we instead recorded the change in TES response for known electrical and optical powers of 50 fW to 70 pW (integration time of 83 ms for both measurements). For input powers of 70 pW to 120 pW, the TES is heated into the upper part of the transition, which has an atypical long tail, where it is much less sensitive.

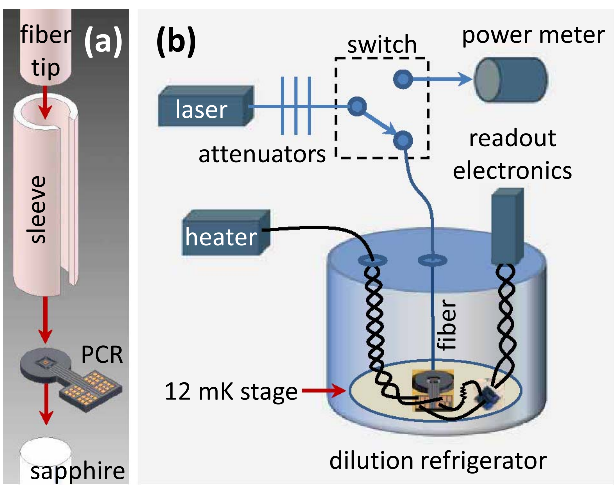

Fig. 2. (Color online) (a) Assembly drawing showing alignment of the fiber core to the center of the radiometer. (b) Simplified schematic of experimental apparatus.

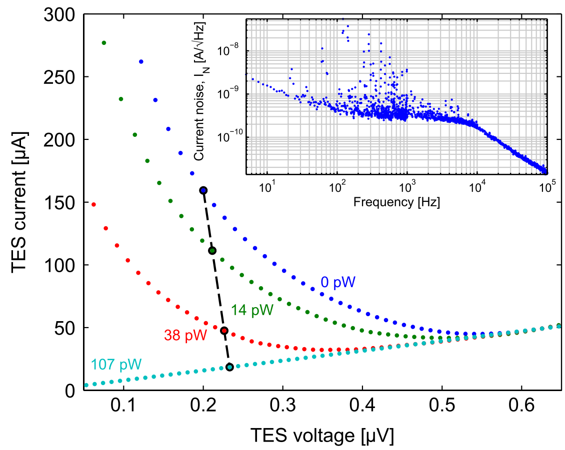

Fig. 3. (Color online) TES I-V curves for a few applied optical powers. The dashed line is the bias used to measure the response to applied electrical and optical powers. Parasitic resistance on the TES bias line caused an additional ≈40 pW stray power for each curve. (Inset) TES current noise versus frequency at zero applied power.

Above 120 pW, the TES is no longer sensitive to temperature.

It is possible to extend the dynamic range of the device by using Johnson noise thermometry (JNT) for higher input powers where the TES is resistive. In this high-power mode, the Johnson current noise generated in the unbiased TES is $\sqrt{4k_BT/R_n}$, where k_B is the Boltzmann constant and T is the TES temperature. We used a signal analyzer to measure the Johnson noise for applied powers of 120 pW to 20 nW. For each applied power, the JNT response is taken to be the average current noise of 100 traces between 2 kHz and 10 kHz. At powers above 20 nW, the Mo wiring leads are driven normal and JNT is no longer sensitive.

The response equivalence is a measure of the equivalence of the device response to absorption of optical power in the absorber versus electrical power dissipated in the heater. The response equivalence is plotted in Fig. 4(a), yielding a mean value of 0.92, meaning that 8% less electrical power is needed to match the response from optical power. Based on a change in absorber appearance after attachment (appears more specular), we attribute the main source of the inequivalence to reflection from the epoxy used to attach the MWCNT absorber.

Because of the large inequivalence compared to metrological-grade absolute CRs, we did not determine the uncertainties in the applied electrical and optical powers. Instead, we used response equivalence measurements to check the noise performance of the device. Using a sliding window (nearest neighbor, 50 points) to find the standard deviation of the response equivalence versus power, we have estimated the power spectral density of the total noise equivalent power (NEP) at 2 Hz [Fig. 4(b)]. The estimate of the total NEP increases with applied optical power due to photon shot noise ($\sqrt{2h\nu P}$) and excess relative intensity noise (RIN, 2.3×10^{-4} P), where P is the applied optical power [13]. The RIN coefficient for the diode laser was estimated using multiple measurements of a photodiode with an integration time of 83 ms. Above

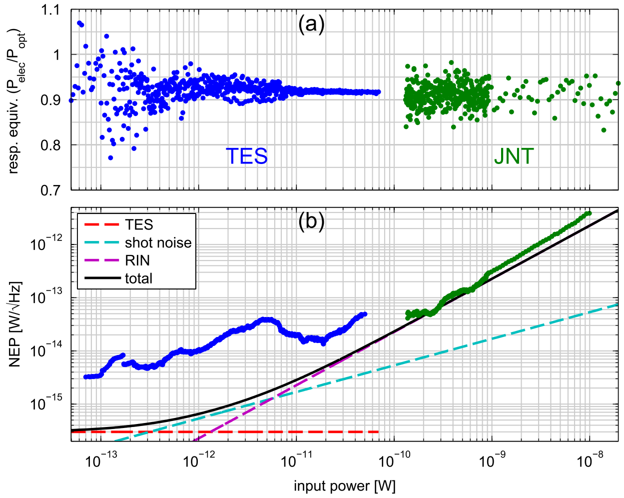

Fig. 4. (Color online) (a) PCR electrical-optical response equivalence versus input power for both TES and JNT modes. (b) Estimated NEP obtained from a sliding window on the data in (a). Dashed lines show NEP theory.

10 pW, our optical measurements are dominated by excess RIN from the laser diode. The TES contribution to the total NEP is $\approx I_N V = 3\times10^{-16}\ \mathrm{W}/\sqrt{\mathrm{Hz}}$, where I_N is the extrapolated current noise at 2 Hz (Fig. 3 inset) and V is the voltage bias (0.2 μV). However, the TES measurements are up to an order of magnitude noisier than expected from our characterization of the device. The excess noise is likely due to excess electrical readout noise at low frequency (sub 2 Hz) in our electronics (amplifier and bias currents), unwanted environmental sources of noise, and temperature drifts due to parasitic heating on the TES bias line.

The theoretical NEP of a TES is dominated by thermal fluctuation noise from the weak thermal link, which is approximately $\sqrt{4k_B T_c^2 G} \simeq 3\times10^{-17}\ \mathrm{W}/\sqrt{\mathrm{Hz}}$ for the current device [14]. We observe a large $1/f$ noise component, which accounts for an order of magnitude degradation from the theoretical limit. However, unlike conventional macroscopic CRs, the time constant of the PCR is much faster, $\approx$100 μs. As a result, instead of operating at 2 Hz, we could operate the system by introducing a modulation scheme to move the measurement frequency above our $1/f$ noise knee and environmental noise sources. In the future, using a stabilized laser and modulation between 100 Hz and 2 kHz, it should be possible to reach measurements of power that are laser shot noise limited down to 4 fW.

The PCR is a new tool that enables the use of conventional radiometric techniques at pW power levels. We have measured the response to optical powers of 50 fW to 20 nW, and a repeatability below $\pm0.3\%$ ($k=2$) for optical powers of 15 pW to 70 pW. We estimate the NEP of our system to be $5\times10^{-15}\ \mathrm{W}/\sqrt{\mathrm{Hz}}$, which is limited by unwanted external noise. However, we believe that with a few straightforward changes in the measurement scheme, it will be possible to eliminate these excess noise sources and achieve a detector-limited NEP of $3\times10^{-17}\ \mathrm{W}/\sqrt{\mathrm{Hz}}$, which is below the shot noise limit even for the lowest powers measured.

References

1. D. J. Livigni, C. L. Cromer, T. R. Scott, B. C. Johnson, and Z. M. Zhang, Metrologia **35**, 819 (1998).
2. J. M. Houston and J. P. Rice, Metrologia **43**, S31 (2006).
3. R. Klein, R. Thornagel, and G. Ulm, Metrologia **47**, R33 (2010).
4. A. J. Miller, A. E. Lita, B. Calkins, I. Vayshenker, S. M. Gruber, and S. W. Nam, Opt. Express **19**, 9102 (2011).
5. C. D. Reintsema, J. A. Koch, and E. N. Grossman, Rev. Sci. Instrum. **69**, 152 (1998).
6. S. I. Woods, S. M. Carr, A. C. Carter, T. M. Jung, and R. U. Datla, Proc. SPIE, **7742**, 77421P (2010).
7. D. J. Livigni, N. A. Tomlin, C. L. Cromer, and J. H. Lehman, Metrologia, **49**, S93 (2012).
8. D. Fukuda, N. Zen, M. Ohkubo, H. Takahashi, K. Amemiya, and M. Endo, IEEE Trans. Instrum. Meas. **56**, 356 (2007).
9. K. D. Irwin, Appl. Phys. Lett. **66**, 1998 (1995).
10. G. C. Hilton, J. M. Martinis, K. D. Irwin, N. F. Bergren, D. A. Wollman, M. E. Huber, S. Deiker, and S. W. Nam, IEEE Trans. Appl. Supercond. **11**, 739 (2001).
11. D. Drung, C. Hinnrichs, and H. J. Barthelmess, Supercond. Sci. Technol. **19**, S235 (2006).
12. J. H. Lehman, M. Terrones, E. Mansfield, K. E. Hurst, and V. Meunier, Carbon **49**, 2581 (2011).
13. P. L. Richards, J. Appl. Phys. **76**, 1 (1994).
14. K. Irwin and G. Hilton, *Transition-Edge Sensors* (Springer-Verlag, 2005).